DOPO-functionalized Fe-based metal–organic framework and its synergistic flame retardant effect with microencapsulated ammonium polyphosphate in epoxy composites

Nhung Hac Thi,[ab] Hong Tham Nguyen,[a] Duc Long Tran,[a] Ho Thi Oanh,[a] Tien Dat Doan,[a] Giang Le Nhat Thuy,[a] Ha Tran Nguyen,[cd] Tuyen Van Nguyen,[ab] and Mai Ha Hoang*[ab]

[a]Institute of Chemistry, Vietnam Academy of Science and Technology, 18 Hoang Quoc Viet, Nghia Do, Ha Noi, 10000, Vietnam

Email: hoangmaiha@ich.vast.vn

[b]Graduate University of Science and Technology, Vietnam Academy of Science and Technology, 18 Hoang Quoc Viet, Nghia Do, Ha Noi, 10000, Vietnam

[c]National Key Laboratory of Polymer and Composite Materials, Vietnam National University Ho Chi Minh City, 268 Ly Thuong Kiet, Dien Hong, Ho Chi Minh City, 70000, Vietnam

[d]Ho Chi Minh City University of Technology, Viet Nam National University-Ho Chi Minh City, 268 Ly Thuong Kiet, Dien Hong, Ho Chi Minh City, 70000, Viet Nam

†Electronic Supplementary Information (ESI) available. See DOI: 10.1039/x0xx00000x

Supporting Information

S1. Experimental

Synthesis of UMF prepolymer

A mixture of 10 g of urea, 10 g of MEL, 50 mL of distilled water, and 10.16 mL of 37% formaldehyde solution was charged into a 500 mL three-neck flask and stirred. The pH of the mixture was adjusted to 8–9 using a 10 wt% Na_2CO_3 solution, followed by heating at 80 °C for 1 h under continuous stirring to obtain a UMF prepolymer solution.

Preparation of APP@UMF

40 g of APP was dispersed in 100 mL of ethanol, followed by the addition of the as-prepared UMF solution under continuous stirring. The mixture was adjusted to pH of 4-5 by 1 M H_2SO_4 solution, and then heated at 80 ^oC for 3 h. The resulting solid was collected by filtration, washed with ethanol, and dried at 80 ^oC for 8 h. The obtained product was denoted as APP@UMF.

S2. Results and Discussion

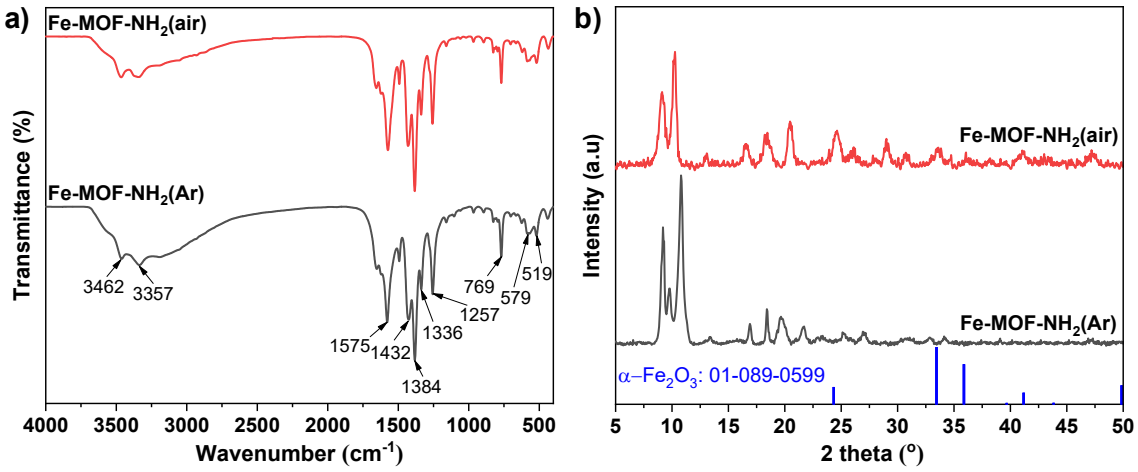

Fig. S1 FT-IR spectra (a) and XRD patterns (b) of Fe-MOF-NH_2(Ar) and Fe-MOF-NH_2(air)

To develop a synthesis route for Fe-BDC-NH_2 MOF that is more suitable for future scale-up, the material was synthesized in a round-bottom flask instead of the conventional Teflon-lined autoclave. Two different reaction atmospheres—air and inert argon—were employed, and the obtained samples were designated as Fe-MOF-NH_2(air) and Fe-MOF-NH_2(Ar), respectively. The FT-IR spectra and XRD patterns of MOFs are shown in Fig. S1. As presented in Fig. S1a, the FT-IR spectra of both samples exhibit similar characteristic absorption bands. Specifically, the peaks at 3462 and 3356 cm^{-1} are assigned to the N–H asymmetric and symmetric stretching vibrations in the amino groups, respectively. The absorption peaks at 1336 and 1257 cm^{-1} correspond to C–N stretching vibrations in aromatic amines, confirming the presence of amino-functionalized ligands. In addition, characteristic peaks at 1575, 1432, and 1384 cm^{-1} are attributed to asymmetric C–O stretching, symmetric C–O stretching, and COO^- vibrations of coordinated carboxylate groups. The bands at 769 and 520-579 cm^{-1} are associated with the C–H bending vibrations of benzene rings and Fe–O stretching modes, respectively.[1-3]

As illustrated in Fig. S1b, the XRD pattern of Fe-MOF-NH_2(Ar) displays the main diffraction peaks at 2θ values of 9.21°, 10.83°, 16.90°, 18.41°, and 19.66°, which are consistent with the crystalline structure of Fe-MOF-NH_2 reported in previous studies,[4, 5] confirming the successful synthesis of the desired MOF phase under an inert atmosphere. For Fe-MOF-NH_2(air), besides the typical reflections of Fe-MOF-NH_2, the XRD pattern of Fe-MOF-NH_2(air) reveals additional peaks at 2θ values of 24.63°, 33.64°, 36.04°, and 41.17°, corresponding to the crystalline planes of α-Fe_2O_3 (ICDD PDF# 01-089-0599). These results indicate that the Fe-MOF-NH_2(air) sample consists of a mixture of Fe-MOF-NH_2 and Fe_2O_3 phases. The formation of Fe_2O_3 impurities is more favorable under air conditions due to the combined effects of Fe^{3+} hydrolysis and oxidative condensation in the presence of dissolved oxygen. Moreover, the amino functionality of $H_2BDC–NH_2$ can locally increase the alkalinity of the reaction medium, further accelerating the hydrolysis of Fe^{3+} ions and facilitating the precipitation of iron oxide species, rather than the coordination-driven assembly of Fe-MOF-NH_2. As a result, carrying out the synthesis under an inert atmosphere is essential to suppress Fe_2O_3 formation and achieve phase-pure Fe-MOF-NH_2 with well-defined crystallinity.

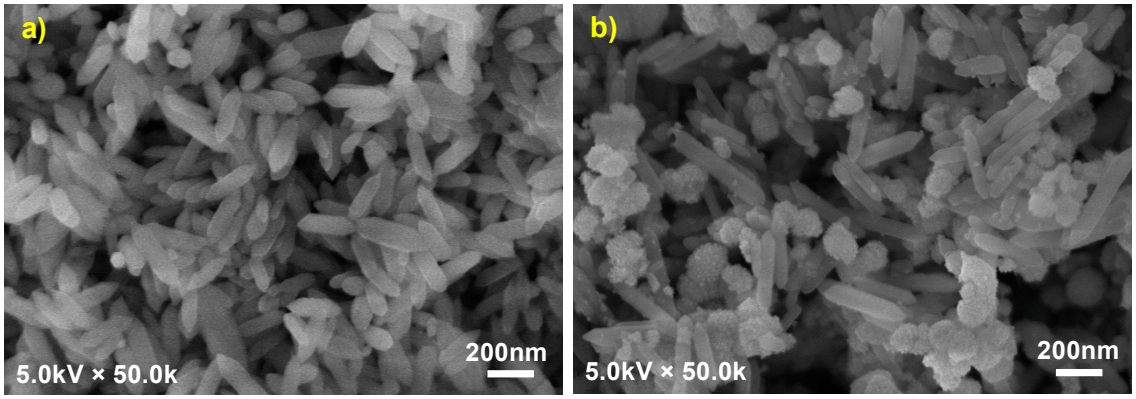

Fig. S2 SEM images of Fe-MOF-NH_2(Ar) (a) and Fe-MOF-NH_2(air) (b)

As shown in Fig. S2a, the Fe-MOF-NH_2(Ar) MOF exhibits a well-defined hexagonal spindle-like morphology, consistent with previous reports.[2, 5, 6] The particle length ranges from 150 to 235 nm, with an average diameter of approximately 60 nm. In contrast, the Fe-MOF-NH_2(air) sample displays a noticeable change in morphology. Although spindle-shaped crystals remain predominant, spherical particles corresponding to α-Fe_2O_3 are also observed. Furthermore, the spindle-like MOF particles in the air-synthesized sample exhibit a significant increase in size, with lengths ranging from 285 to 510 nm and an average diameter of about 65 nm (Fig. S2b). These observations are in good agreement with the XRD analysis discussed above. Taken together with the XRD results, it can be concluded that maintaining an inert atmosphere during synthesis is indispensable for achieving high-purity Fe-MOF-NH_2.

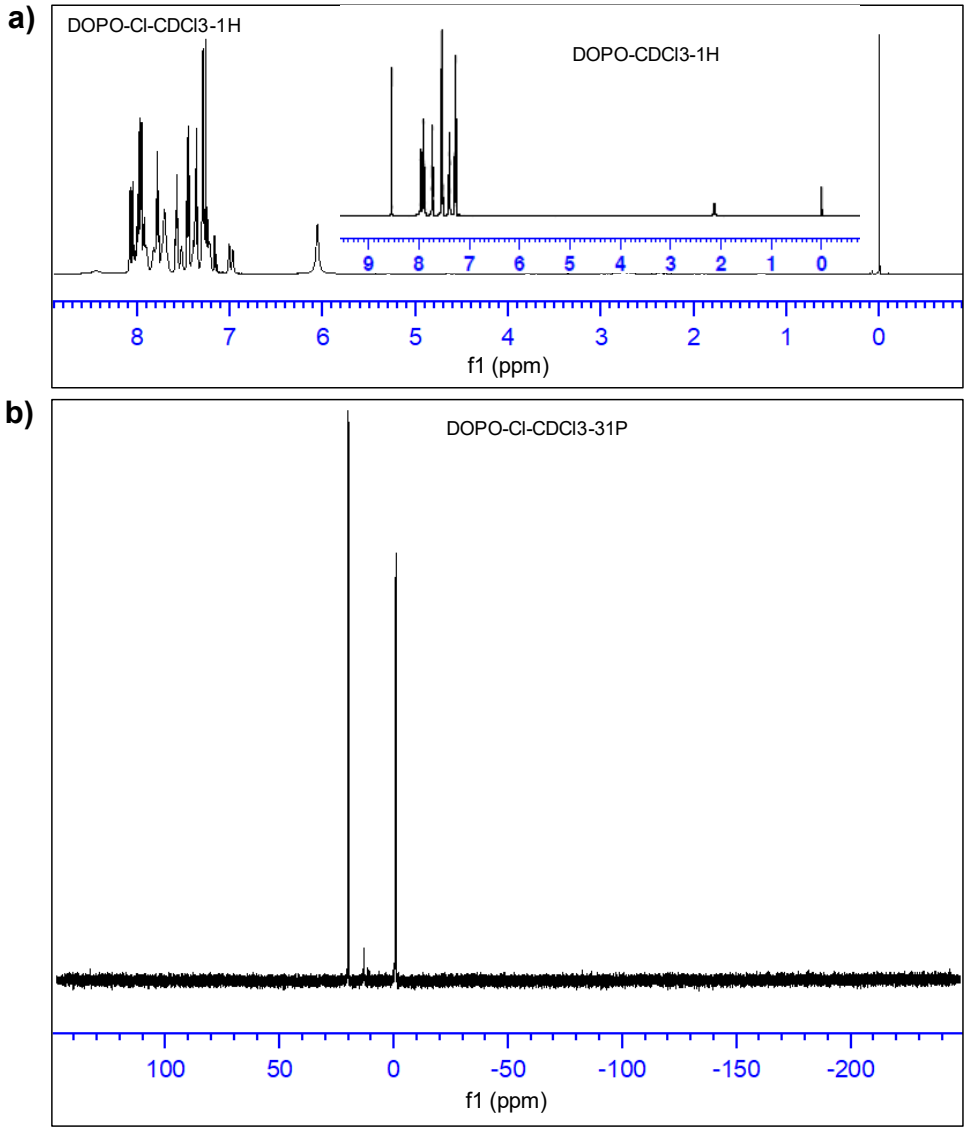

Fig. S3 ^{1}H NMR spectrum (600 MHz, $CDCl_3$) (a) and ^{31}P NMR spectrum (243 MHz, $CDCl_3$) (b) of DOPO-Cl sample without purification. Inset Figure in Fig. S3a is ^{1}H NMR spectrum (600 MHz, $CDCl_3$) of DOPO

The ^{1}H NMR spectra of DOPO and DOPO-Cl are displayed in Fig. S3a. The ^{1}H NMR of DOPO-Cl sample exhibits characteristic aromatic proton signals. Notably, compared with DOPO, the signal at δ 8.53 ppm disappears in the spectrum of DOPO-Cl, indicating the transformation of the P-H bond to the P-Cl bond. Furthermore, the ^{31}P NMR spectrum of DOPO-Cl appears a signal at δ 20.0 ppm (Fig. S3b), demonstrating the formation of the P-Cl bond, which is consistent with the previous report.[7] These results confirm the successful synthesis of DOPO-Cl.

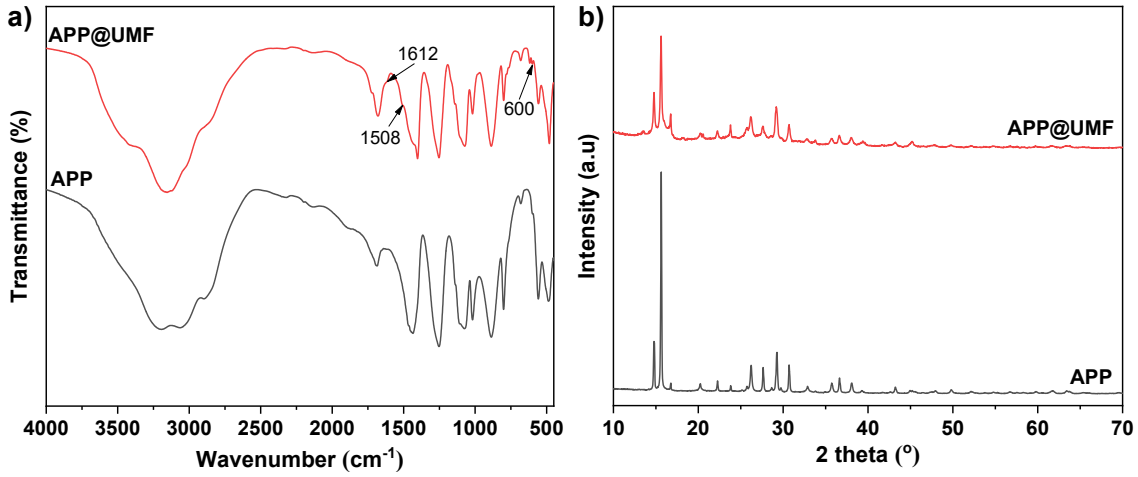

Fig. S4 FT-IR spectra (a) and XRD patterns (b) of APP and APP@UMF

The FT-IR spectra and XRD patterns of APP and APP@UMF are depicted in Fig. S4. As shown in Fig. S4a, the characteristic absorption bands of APP observed at 3196 (N–H stretching), 1252 (P=O stretching), 1081 and 890 (symmetric and asymmetric P–O stretching), 1020 (symmetric P–O vibrations in PO_2 and PO_3 groups), and 800 cm^{-1} (P–O–P vibrations),[8, 9] appear in both FT-IR spectra. Additionally, the FT-IR spectrum of APP@UMF exhibits new peaks at 1612 (C=O stretching in –N–(CO)–N–), 1508 (C–N stretching), and 600 cm^{-1} (triazine ring vibrations).[8-10] These results demonstrate the coexistence of APP and UMF resin in the APP@UMF sample.

As observed in Fig. S4b, both APP and APP@UMF display similar diffraction patterns, indicating that the crystalline structure of APP is retained after modification. However, the diffraction intensity of APP@UMF decreases noticeably compared with that of pristine APP. This reduction in peak intensity suggests that the surface of APP is partially covered by the amorphous UMF resin, which weakens the overall crystallinity of the material. The absence of new diffraction peaks further confirms that no new crystalline phase is formed during the coating process. These results, in combination with the FT-IR analysis, demonstrate the successful incorporation of UMF resin onto the APP surface.

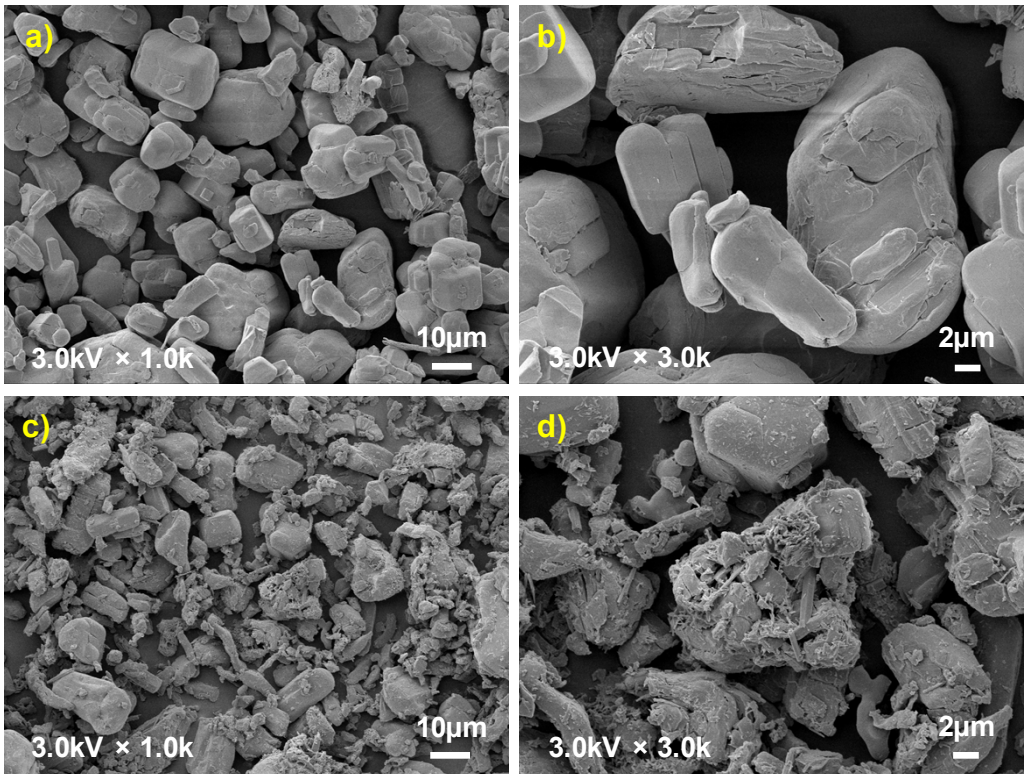

Fig. S5 SEM images of APP (a, b) and APP@UMF (c, d) at different magnifications

Fig. S5 shows the surface morphologies of APP and APP@UMF. As shown in Fig. S5a and S5b, pristine APP particles exhibit smooth surfaces. In contrast, after modification, the surface of APP becomes noticeably rougher (Fig. S5c and S5d). This distinct morphological change reveals that APP particles are well-coated with the UMF resin layer, which is consistent with the above FT-IR and XRD results.

References

1. A. D. S. Barbosa, D. Julião, D. M. Fernandes, A. F. Peixoto, C. Freire, B. de Castro, C. M. Granadeiro, S. S. Balula and L. Cunha-Silva, *Polyhedron*, 2017, **127**, 464–470.

2. K. Vinothkumar and R. G. Balakrishna, Applied Catalysis B: Environmental, 2024, **340**, 123199.

3. L. Meng, Z. Zhang, M. Ju, J. Xu and Z. Wang, *International Journal Energy Research*, 2022, 1–13.

4. X.-X. Zheng, L.-J. Shen, X.-P. Chen, X.-H. Zheng, C.-T. Au and L.-L. Jiang, *Inorganic Chemistry,* 2018, **57**, 10081–10089.

5. S.-W. Lv, J.-M. Liu, C.-Y. Li, N. Zhao, Z.-H. Wang and S. Wang, *Chemical Engineering Journal*, 2019, **375**, 122111.

6. L. Larasati, D. Dendy, W. W. Lestari, R. S. R. Suharbiansah, M. Firdaus, A. Masykur and F. R. Wibowo, *Journal of Inorganic and Organometallic Polymers and Materials*, 2024, 34, 4039–4049.

7. A. K. Salmeia, G. Baumgartner, M. Jovic, A. Gössi, W. Riedl, T. Zich and S. Gaan, *Organic Process Research & Development*, 2018, **22**, 1570–1577.

8. K. Wu, Z. Wang and Y. Hu, *Polymers for Advanced Technologies*, 2008, **19**, 1118–1125.

9. W Wang, W. Zhang, S. Zhang and J. Li, *Construction and Building Materials*, 2014, 65, 151-158.

10. A. M. Bakry, F. S. Awad, J. A. Bobb, A. A. Ibrahim and M. S. El-Shall, *RSC Advances*, 2020, **10**, 37883.